Available online at www.eccomasproceedia.org
Eccomas Proceedia SMART (2023) 11-22

ECCOMAS
Proceedia

X ECCOMAS Thematic Conference on Smart Structures and Materials
SMART 2023
D.A. Saravanos, A. Benjeddou, N. Chrysochoidis and T. Theodosiou (Eds)

CALCULATION OF THE SWITCHING FIELD FOR MAGNETIC SHAPE MEMORY ALLOYS USING FINITE ELEMENT ANALYSIS

Aleksandr Nemov[1], Andrey Saren[2], Marko Matikainen[1], Kari Ullakko[2], and Aki Mikkola[1]

[1]Department of Mechanical Engineering
LUT University
Yliopistonkatu 34, 53850, Lappeenranta, Finland
e-mail: aleksandr.nemov@lut.fi

[2] Material Physics Laboratory
LUT University
Yliopistonkatu 34, 53850, Lappeenranta, Finland

Abstract. Magnetic shape memory (MSM) alloys are among the most promising smart materials, capable of revolutionizing several multidisciplinary areas, such as soft robotics, digital hydraulics, and multiple biomedical applications. The characteristic aspect of the MSM effect is structure reorientation in a martensite of MSM alloy, associated with the movement of the twin boundary (TB), the interface between differently oriented martensite variants. Even though the MSM effect has been under investigation since its discovery in 1996, there is still plenty of controversy in theoretical predictions based on different assumptions. In our research, we investigated one of the fundamental aspects of the MSM effect – conditions for setting a (TB) in motion. The effect was analyzed for a two-variant specimen of five-layered modulated martensite of Ni-Mn-Ga with a single TB. Three-dimensional finite element analysis of magnetic field was employed, and energy-based criteria for setting the TB in motion was applied, using the results of magnetic field calculation. Results of the simulation study were compared with experimentally determined magnitude of the magnetic field required for initiating the TB movement in the considered specimen, and applicability of the used assumptions was assessed. Findings of the study clarify the role of three-dimensional non-homogeneous distribution of magnetic field across the TB, which is usually not accounted for in theoretical models of the MSM effect. Ways of further development of the approach for the simulation-based prediction of the switching field are proposed.

Key words: Finite Element Analysis, Magnetic Shape Memory Alloy, Switching Field, Twin Boundary

Peer-review under responsibility of the organizing committee of SMART 2023.
doi: 10.7712/150123.9760.445291

1 INTRODUCTION

The Magnetic Shape Memory (MSM) effect as a phenomenon of large magnetic field-induced strains was first observed by Prof. Kari Ullakko in 1996 [1] and has been the subject of extensive scientific research ever since. The effect is based on the existence of structural twin variants with different crystal orientations, separated from each other by twin boundaries (TB). Under the action of external factors (magnetic field and/or mechanical loads), variants that are favourably oriented with respect to the external conditions, can grow at the expense of other variants. The process is associated with the movement of the TB inside the specimen and can produce giant strains.

A large number of methods for modelling the MSM effect have been proposed, including phenomenological models [2, 3], constitutive models based on internal parameters representing the averaged state of the alloy microstructure [4, 5, 6], and micromagnetics modelling [7, 8].

Most studies on the MSM effect [5, 9, 10, 11] attribute TB movements to magnetostress that can be calculated using the difference in free energy across the TB. Different studies, however, adopt different approaches to calculating that difference in the free energy across the TB, which leads to significantly different numerical results.

Analytical estimations can be made for the Zeeman and anisotropy components of the free energy [12]. The stray field was not accounted for in this approach, and the total difference in the free energy across the TB was calculated using the Zeeman and anisotropy contributions. Using the expressions derived in [12], we can estimate the difference in the free energy between the easy-variant and the hard-variant per unit volume ΔE as:

$$\Delta E = \begin{cases} -K_u(1\eta - \eta^2), & \text{if } \eta \leq 1 \\ -K_u, & \text{if } \eta > 1 \end{cases}, \quad \eta = \frac{M_s H}{2K_u}, \tag{1}$$

where K_u is the anisotropy constant, H is the applied magnetic field, and M_S is the saturation magnetization.

In this study, we performed 3D calculations of the magnetic state of a specimen with a single twin boundary, and used those calculation results to estimate the free energy and the magnetostress as a driving force for the TB motion.

2 SIMULATION APPROACH

We consider the following components of the free energy in a MSM alloy: Zeeman energy, magnetocrystalline anisotropy energy, and stray field energy. Some studies [7, 8] account also for the exchange energy, which is responsible for the formation of $180°$-domains. This energy, however, is determined by the exchange constant, which is not available for a material under consideration. Also, the movement of $180°$-domains boundaries does not cause the movement of the TB and is, therefore, not relevant for this study.

The considered three components of the free energy are determined as follows.

2.1 Free energy calculations

2.1.1 Zeeman energy

The Zeeman energy is defined by the external magnetic field $\mathbf{H_{ext}}$ and the induced magnetization $\mathbf{M}$ of the ferromagnetic material. It does not account for the field generated by the magnetization. The Zeeman energy density (energy per unit volume) is:

$$E_{Zeeman} = -\mu_0 \mathbf{M} \cdot \mathbf{H_{ext}}, \tag{2}$$

where $\mu_0 \approx 1.257 \cdot 10^{-6}\ \mathrm{NA}^{-2}$ is the vacuum permeability.

2.1.2 Magnetocrystalline anisotropy energy

The magnetic anisotropy energy density is defined by the angle γ between the magnetization vector $\mathbf{M}$ and the axis of easy magnetization (c-axis):

$$E_{anisotropy} = K_u \sin^2 \gamma, \tag{3}$$

where K_u is the anisotropy constant.

2.1.3 Stray field (internal field) energy

The magnetic field inside a ferromagnetic region is in fact different from the one externally applied, because the induced magnetization produces its own (internal, or stray) magnetic field $\mathbf{H_d}$. The field $\mathbf{H_d}$ is defined by the differential Maxwell equations and in general case cannot be estimated analytically. The energy per unit volume associated with this field is:

$$E_{stray} = -\frac{\mu_0}{2} \mathbf{M} \cdot \mathbf{H_d}. \tag{4}$$

2.2 Magnetic fields in the finite element simulations

When solving the Maxwell equations for electromagnetic fields, the magnetization vector is not necessarily used in the finite element (FE) analysis explicitly. Instead, when solving Maxwell equations, a $B-H$ curve is used as a constitutive equation for a ferromagnetic region. In our study, we used two $B-H$ curves measured for easy and hard directions of magnetization, i.e., along and perpendicular to the easy magnetization c-axis. After finding a solution for the magnetic field, the magnetization vector at any point can be found:

$$\mathbf{B} = \mu_0 (\mathbf{H} + \mathbf{M}) \quad \Rightarrow \quad \mathbf{M} = \frac{1}{\mu_0} \mathbf{B} - \mathbf{H} \tag{5}$$

Also, the fact that the resulting $\mathbf{B}$ and $\mathbf{H}$ satisfy Maxwell equations accompanied by the provided $B-H$ curves for ferromagnetic materials, implies that $\mathbf{H}$ in the solution is an effective magnetic field that already includes the demagnetizing field $\mathbf{H_d}$.

$$\mathbf{H} = \mathbf{H_{ext}} + \mathbf{H_d} \quad \Rightarrow \quad \mathbf{H_d} = \mathbf{H} - \frac{1}{\mu_0}\mathbf{B_{applied}} \tag{6}$$

Using the magnetization vector $\mathbf{M}$ found according to Eq. 5 and the demagnetizing field found according to 6, the Zeeman, stray, and anisotropy components of the free energy can be found as described above.

2.3 Finite element model of a specimen for magnetic field calculation

We consider a specimen of Ni-Mn-Ga alloy with a rectangular $1\,\mathrm{mm} \times 1\,\mathrm{mm}$ cross-section. The sketch of the specimen consisting of two martensite variants with a single TB separating them from each other is shown in Fig. 1. The red c arrow in Fig. 1 indicates the direction of the easy axis of magnetization in the considered variants.

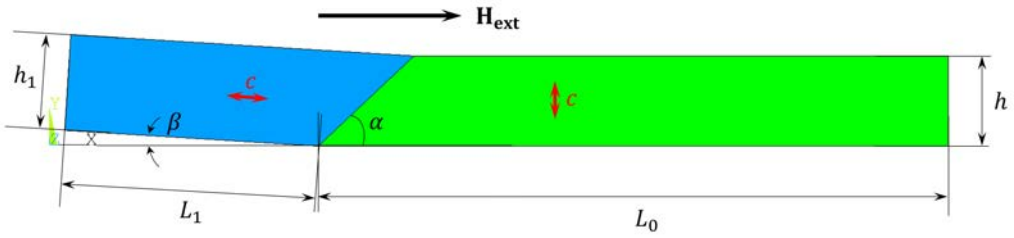

Figure 1: Two-variant Ni-Mn-Ga specimen with a single TB

In our study we consider external field $\mathbf{H_{ext}}$ applied along the long side of the specimen (axis X in Fig. 1). With respect to that field, the variant of length L_0 pictured with green color will be referred to as hard-variant, whereas the variant of length L_1 shown with blue color will be referred to as easy-variant.

The twin boundary, separating two variants, is inclined by the angle α determined by the crystalline lattice parameters c and a:

$$\alpha = \arctan\left(\frac{c}{a}\right) \tag{7}$$

The easy-variant part of the specimen is inclined by the angle β:

$$\beta = \frac{\pi}{2} - \alpha \tag{8}$$

In the presented simulations we consider the following parameters of the Ni-Mn-Ga specimen:

$$\frac{c}{a} = 0.94; \quad L = 10\,\mathrm{mm}; \quad L_0 = 7\,\mathrm{mm}; \quad h = 1\,\mathrm{mm}. \tag{9}$$

The following magnetic properties were used for the Ni-Mn-Ga alloy [13]: Saturation magnetization $\mu_0 M_s = 0.705\,\mathrm{T}$; anisotropy field $H_a = 560\,\mathrm{kA/m}$; anisotropy constant $K_u =$

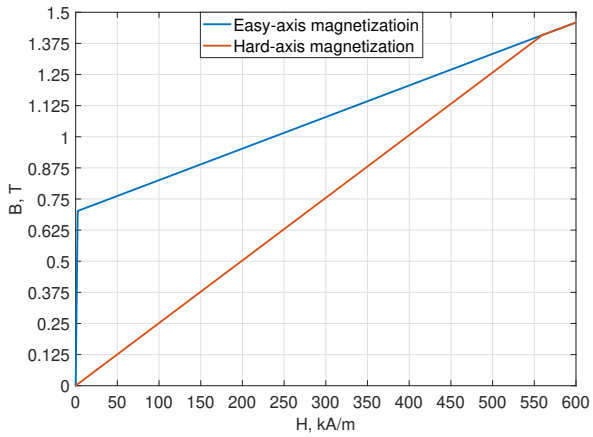

Figure 2: $B - H$ curves used for the directions of easy and hard magnetization [13]

$196\,\mathrm{kJ/m^3}$. The $B - H$ dependencies assumed for the easy and hard directions [13] are presented in Fig. 2.

A 3D FE model of the two-variant specimen is shown in Fig.3. While the considered specimen has a cross section of $1\,\mathrm{mm} \times 1\,\mathrm{mm}$ and the length $10\,\mathrm{mm}$, the dimensions of the computational domain were chosen as $3\,\mathrm{mm} \times 3\,\mathrm{mm} \times 12\,\mathrm{mm}$, which approximately corresponds to the typical dimensions of solenoids used in experimental studies. The mesh was made in a way that at the TB location the element size is $\sim 15\,\mu\mathrm{m}$ in all dimensions. That element size was identified in a convergence study and proved to ensure accuracy about 0.1% in calculation of the magnetic flux density at the TB for the considered external fields. The dimensions of a single finite element near the TB are approximately one order of magnitude larger than characteristic dimensions of material samples typically analyzed in micromagnetic simulations [7, 8].

ANSYS code and the finite element formulation based on magnetic vector potential $\mathbf{A}$ was used for solving the magnetostatic problem:

$$\mathbf{B} = \nabla \times \mathbf{A} \tag{10}$$

For boundary conditions, a linear distribution of the magnetic vector potential $\mathbf{A}$ components corresponding to the given magnetic flux density $\mathbf{B_{applied}}$ was prescribed. The external magnetic field $\mathbf{H_{ext}}$ can be therefore found as

$$\mathbf{H_{ext}} = \frac{1}{\mu_0}\mathbf{B_{applied}} \tag{11}$$

3 RESULTS AND DISCUSSION

3.1 Field distribution

As a result of the FE analysis performed for each value of the applied external field $\mathbf{B_{applied}}$ ($\mathbf{H_{ext}}$), a distribution of the magnetic flux density $\mathbf{B}$ in the specimen was obtained. An example

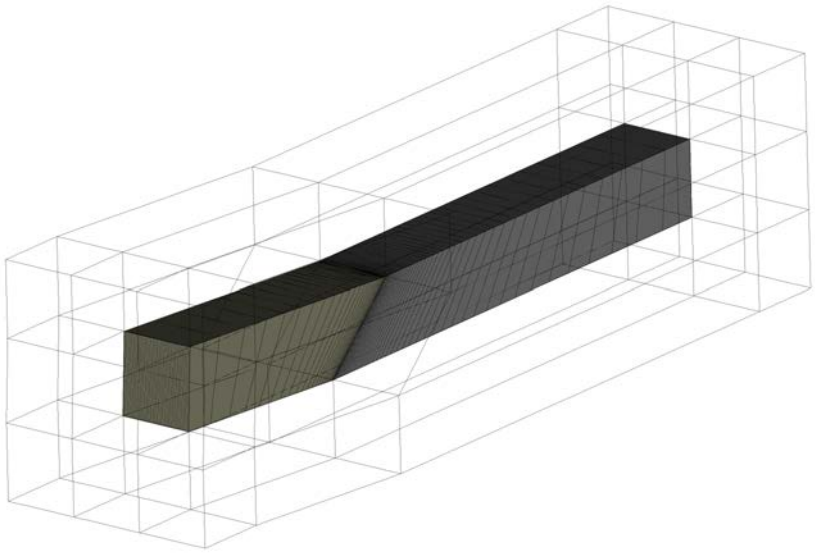

Figure 3: FE model of a Ni-Mn-Ga specimen with a single TB

of the B field distribution for the applied field 0.2 T is presented in Fig. 4

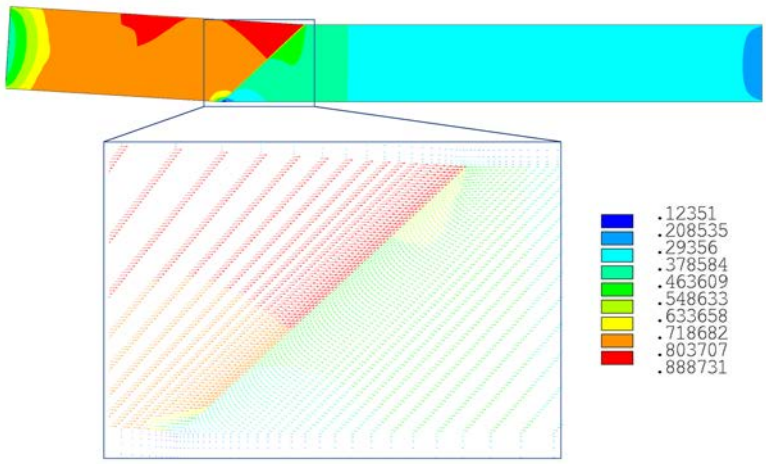

Figure 4: Magnetic flux density inside the Ni-Mn-Ga specimen for the applied external field 0.2 T, T

3.2 Free energy

Using the results of the FE simulation described above, the free energy components can be calculated in the elements adjacent to the TB and belonging to both martensite variants according to Eq. (2), (3), and (4). A numerical procedure was implemented to calculate the difference between the energy values in two variants at each point of the TB. The calculated distributions of the the free energy components differences for the applied external field of

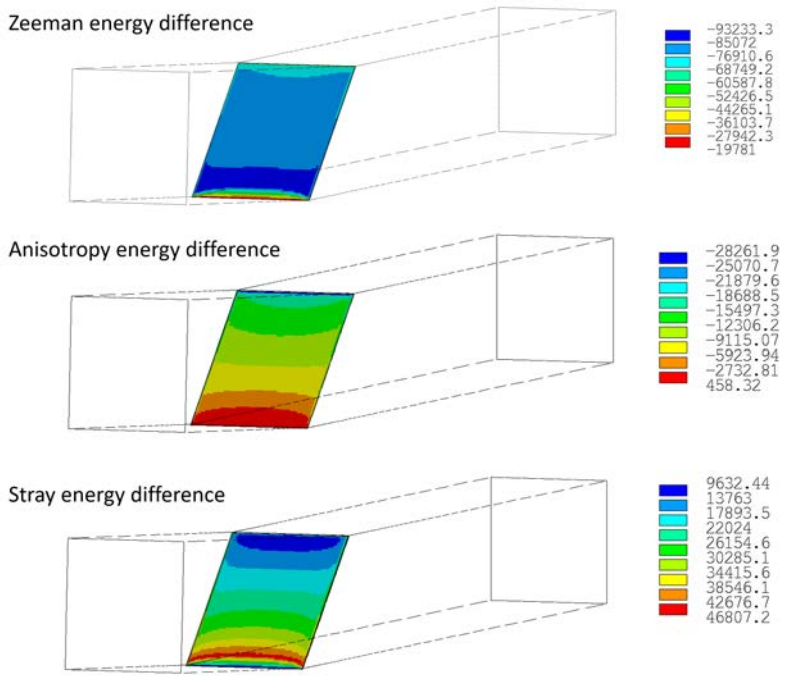

Figure 5: Difference of the free energy components across the TB for the applied external field $0.2\,\mathrm{T}$, J/m^3

$0.2\,\mathrm{T}$ are shown in Fig. 5.

Fig. 5 illustrates significantly non-homogeneous distribution of the energy differences across the TB, which can only be obtained in 3D analysis and is usually neglected. In particular, while the non-homogeneity for the Zeeman energy is moderate (the values are within 20% of the average value except for the small areas at the top and bottom sides of the specimen), the anisotropy energy difference changes almost linearly from 0 on the bottom side to the values above $20\,\mathrm{kJ/m^3}$ on the top side. That yields significant heterogeneity of the full free energy difference distribution – the values vary approximately 4 times withing the TB for the applied field $0.2\,\mathrm{T}$. That means also a non-homogeneous distribution of the magnetostress across the TB, which may strongly affect the value of the switching field, setting the TB in motion.

It is customary to consider the total force produced by the magnetostress as a factor responsible for setting the TB in motion. According to that, an averaging procedure was applied to the non-homogeneous distributions of the difference in the free energy between the easy- and hard-variants. Area averaging was implemented by considering the free energy values at each finite element, multiplying them by the area of the TB occupied by the corresponding element, summing over all elements adjacent to the TB, and dividing by the total TB area. The comparison of the free energy components difference between two variants at the TB (averaged across the TB values) obtained by 3D FE simulations and analytically with Eq. 1, is shown in Fig. 6. The results based on 3D FE analysis and on analytical estimations illustrate qualitatively very similar behaviour. However, while for strong fields the results are also quite close quantitatively, for low fields below $50\,\mathrm{kA/m}$ the difference between these two sets of results is high. Possible

reasons for that will be discussed below in connection to the switching field calculation.

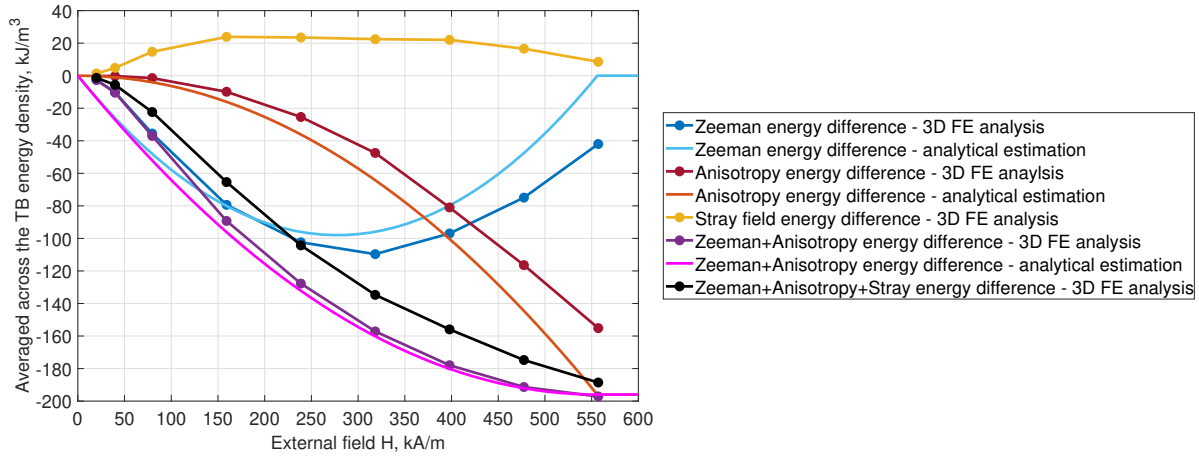

Figure 6: Difference in the free energy across the TB, comparison of numerical 3D FE simulations and analytical estimations

3.3 Driving force for the TB motion

Magnetostress considered a driving force for the TB motion, can be calculated using the difference in the free energy across the TB [10, 14]:

$$\sigma_{mag} = \frac{|\Delta E|}{\epsilon_0}, \tag{12}$$

where $\Delta E = \Delta E_{Zeeman} + \Delta E_{anisotropy} + \Delta E_{stray}$ is the difference in the full free energy across the TB, and $\epsilon_0 = 1 - {}^{c}/_{a}$ is the strain associated with twinning transformation between two variants. Using the magnetostress calucalted with Eq.12, the condition for setting the TB in motion can be formulated as

$$\sigma_{\mathbf{mag}} \geq \sigma_{tw}, \tag{13}$$

where σ_{tw} is the twinning stress for the martensite under consideration.

It has been demonstrated that in Ni-Mn-Ga alloys two crystallographically different types of twin boundaries are possible [15, 14]. These two types are referred to as Type-I and Type-2 boundaries, and are characterized by significantly different values of the switching field [15, 13]. By postprocessing experimental curves measured in [13], we conclude that for the considered alloy the twinning stress for Type-I boundary is $0.5 \pm 0.1\,\mathrm{MPa}$, and for Type-II boundary $0.09 \pm 0.01\,\mathrm{MPa}$. At the same time, experimentally obtained values for the switching field [13] are $50\,\mathrm{kA/m}$ for Type-I boundary, and $14\,\mathrm{kA/m}$ for Type-II. Table 1 presents the comparison of experimental data, data based on the 3D FE analysis and the analytical approach, Eq.1. Since in the FE analysis the data was obtained only at discrete points, a parabolic fit was used to interpolate for the switching field values

Table 1: Switching field, free energy difference and magnetostress for Type-I and Type-II boundaries

Field, kA/m	ΔE, $\mathrm{J/m^3}$ 3D FE	σ_{mag}, MPa 3D FE	ΔE , $\mathrm{J/m^3}$ Analytics	σ_{mag}, MPa Analytics	σ_{tw}, MPa Experiment
14	-722	0.012	-9899	0.165	0.09 ± 0.01 (TB of Type-II)
50	-8851	0.148	-33523	0.559	0.5 ± 0.1 (TB of Type-I)

The data presented in Table 1 show that estimation of the magnetostress using the free energy difference from 3D FE analysis leads to significantly lower value of magnetostress in comparison with simple analytical estimation, and the difference is even higher for lower applied field associated with the movement of highly mobile Type-II boundary. At the same time, the considered simple analytical estimations based purely on $B - H$ curves for single-variant states of the martensite, are in a relatively good correlation with experimental observations. Similarly, for a given value of the twinning stress, the 3D FE approach leads to significantly overestimated values of the switching field. As can be seen from Fig. 6, the significant difference in 3D FE simulations and analytical estimation for low values of external field is mostly because of the different results for the Zeeman energy difference across the TB. While in analytical estimation for small values of the applied field, the Zeeman energy difference grows almost linearly with the external field, the finite element analysis gives much lower values for it. There are several factors that contribute to this difference.

1. In the results of 3D FE analysis, the magnetization $\mathbf{M}$ magnitude in the easy-variant is for the significant part of the TB lower than the saturation value M_s. That can be interpreted as presence of $180°$-domains with opposite orientation of the magnetization in the easy-variant. The analytical estimation, on the contrary, is based on the assumption that saturation has been achieved in the easy-variant for any considered external fields (therefore resulting in an almost linear growth of the Zeeman energy difference with the external field). It is likely that real distribution of $180°$-domains in the easy-variant in the area close to the TB for very small values of external field is quite complicated, and accounting for micromagnetics is necessary to obtain it in the simulations. In order to estimate the influence of this factor, we repeated the calculations using the saturation value M_s for the magnitude of the magnetization in the easy-variant, similarly to how it is assumed in analytical estimations. However, in contrast to the analytical approach, the magnetization in the hard-variant was obtained from FE magnetostatic simulations, and the stray field energy was accounted for. Results of this calculation in comparison with analytical estimation are shown in Fig. 7. As follows from Fig.7, modifying the approach to calculating the Zeeman energy in the easy-variant made results very close to the analytical ones for weak external fields. Moreover, it can be noted that the sum of differences in the Zeeman and anisotropy energies is now virtually indistinguishable from the analytical results, even though the values for the Zeeman energy and for the anisotropy energies itself in the FE calcu-

lations and in the analytical estimation differ significantly for strong external fields. Prediction of the switching field using this approach apparently leads virtually the same results as when using the analytical estimations, but for stronger external fields, due to accounting for the stray energy in FE calculations, the results differ noticeably.

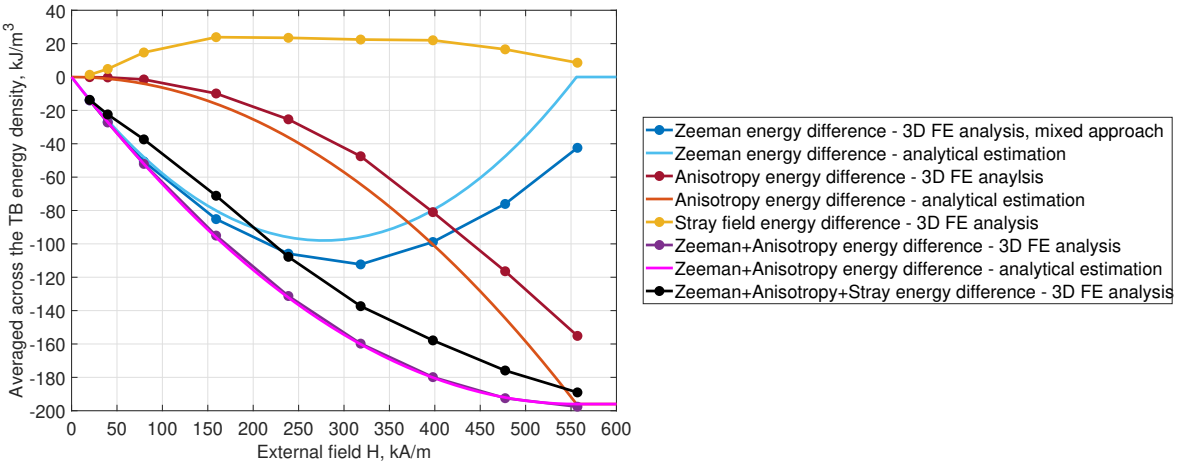

Figure 7: Difference in the free energy across the TB, comparison of numerical 3D FE simulations and analytical estimation. Assumption of saturated magnetization value in the easy-variant when calculating the Zeeman energy in 3D FE simulations

2. In the adopted FE approach, in order to simulate external magnetic field, a distribution of the magnetic vector potential was prescribed at the external boundary of the computational domain. The size of this domain was chosen so as to represent typical dimensions of a solenoid used to generate the external field in experiments [13]. However, our study showed that for relatively low values of the external field this approach leads to results that depend significantly on the chosen size of the computational domain because of the complex configuration of the demagnetizing field. In particular, increasing the size of the computational domain two times lead to an increase in the Zeeman energy difference by a factor of 1.5, making the simulation results somewhat closer to the experimental data. Prescribing the external field extremely far from the specimen, however, does not really match the experimental conditions. A better way to make the external field in 3D FE calculations match the field in the experiment would be including the solenoid used in the experimental setup in the simulations explicitly.

3. The force interaction between two variants in the considered two-variant configuration was not accounted for in the presented simulations. Because of the induced magnetization, the attraction force between two variants may influence the switching field. This term was accounted for in the analytical modelling presented in [16], and allowed to obtain much closer results for the switching field than the simplified analytical approach used for comparison in our study. The influence of this factor in connection with using 3D FE analysis should be investigated additionally.

4 CONCLUSIONS

In the present study, we used 3D finite element analysis for magnetostatic calculations for a two-variant Ni-Mn-Ga specimen with a single TB. Results of the 3D FE analysis were used for calculating the difference between the free energy in two variants at the TB, and a prediction of the switching field for the MSM alloy was made. Results show significant difference with analytical estimations that are often used, especially for the low strength of the external field. Additionally, results demonstrate strongly non-homogeneous distribution of the free energy across the TB, which cannot be obtained in analytical estimations and may influence the TB movement. While qualitatively the dependence of the averaged across the TB values of the free energy on the external field is similar with the analytical one, the adopted approach provides significantly overestimated values for the switching field that do not correlate well with existing experimental data. Three different factors contributing to this difference were identified, and the additional study conducted to estimate their influence suggests possible ways of improving the model and ensuring better correlation with the experimental data.

Acknowledgements

The authors would like to thank the Academy of Finland (grants No. 325911 and 349579) for the funding that made this work possible.

REFERENCES

[1] K. Ullakko, J. K. Huang, C. Kantner, and R. C. O. Handley, "Large magnetic-field-induced strains in Ni_2MnGa single crystals," *Appl. Phys. Lett.*, vol. 69, pp. 1966–1968, 1996.

[2] F. Auricchio, A.-L. Bessoud, A. Reali, and U. Stefanelli, "A phenomenological model for the magneto-mechanical response of single-crystal magnetic shape memory alloys," *European Journal of Mechanics, A/Solids*, vol. 52, pp. 1–11, 2015.

[3] J. Ziske, F. Ehle, H. Neubert, A. Price, and J. Lienig, "A simple phenomenological model for magnetic shape memory actuators," *IEEE Transactions on Magnetics*, vol. 51, no. 1, p. art. 6853406, 2015.

[4] L. Hirsinger and C. Lexcellent, "Internal variable model for magneto-mechanical behaviour of ferromagnetic shape memory alloys Ni-Mn-Ga," *Journal De Physique. IV : JP*, vol. 112, no. II, pp. 977–980, 2003.

[5] J. Wang and P. Steinmann, "Finite element simulation of the magneto-mechanical response of a magnetic shape memory alloy sample," *Philosophical Magazine*, vol. 93, no. 20, pp. 2630–2653, 2013.

[6] M. Mousavi and J. Arghavani, "A three-dimensional constitutive model for magnetic shape memory alloys under magneto-mechanical loadings," *Smart Materials and Structures*, vol. 26, no. 1, p. art. 015014, 2017.

[7] A. Hobza and P. Müllner, "Magnetic torque in single crystal ni–mn–ga," *Shape Memory and Superelasticity*, vol. 3, no. 2, pp. 139–148, 2017.

[8] M. Veligatla, C. Titsch, W.-G. Drossel, C. Garcia-Cervera, and P. Müllner, "Sensitivity of twin boundary movement to sample orientation and magnetic field direction in Ni-Mn-Ga," *Acta Materialia*, vol. 186, no. 2, pp. 389–395, 2020.

[9] P. Müllner and K. Ullakko, "The force of a magnetic/electric field on a twinning dislocation," *Physica Status Solidi (B) Basic Research*, vol. 208, no. 1, pp. R1–R2, 1998.

[10] A. Likhachev and K. Ullakko, "Magnetic-field-controlled twin boundaries motion and giant magneto-mechanical effects in Ni-Mn-Ga shape memory alloy," *Physics Letters, Section A: General, Atomic and Solid State Physics*, vol. 275, no. 1-2, pp. 142–151, 2000.

[11] K. Haldar, D. Lagoudas, and I. Karaman, "Magnetic field-induced martensitic phase transformation in magnetic shape memory alloys: Modeling and experiments," *Journal of the Mechanics and Physics of Solids*, vol. 69, no. 1, pp. 33–66, 2014.

[12] M. Marioni, R. O'Handley, and S. Allen, "Pulsed magnetic field-induced actuation of Ni–Mn–Ga single crystals," *Applied Physics Letters*, vol. 83, no. 19, pp. 3966– 3968, 2003.

[13] A. Saren, "Twin boundary dynamics in magnetic shape memory alloy Ni-Mn-Ga five-layered modulated martensite," *LUT University. Acta Universitatis Lappeenrantaensis 829*, 2018.

[14] O. Heczko, "Magnetic shape memory effect and highly mobile twin boundaries," *Materials Science and Technology (United Kingdom)*, vol. 30, no. 13, pp. 1559 – 1578, 2014.

[15] L. Straka, H. Hänninen, and O. Heczko, "Temperature dependence of single twin boundary motion in Ni-Mn-Ga martensite," *Applied Physics Letters*, vol. 98, p. art. no. 141902, 2011.

[16] O. Heczko, D. Vokoun, V. Kopecky, and B. M., "Effect of magnetostatic interactions on twin boundary motion in Ni-Mn-Ga magnetic shape memory alloy," *IEEE Magnetics Letters*, vol. 6, p. art. no. 7132713, 2015.